Supporting Information for:

Capillary Pressure–Saturation Relations for Supercritical CO_2 and Brine in Limestone/Dolomite Sands: Implications for Geologic Carbon Sequestration in Carbonate Reservoirs

Shibo Wang and Tetsu K. Tokunaga
Earth Sciences Division, Lawrence Berkeley National Laboratory
1 Cyclotron Road, Berkeley, California 94720, USA

Environmental Science and Technology

14 pages

Table of Contents

1 Porous Media

Moderate-sized granular limestone (with 0.1–1.0 percent (wt/wt) quartz, density of 2.71 g/cm^3; Specialty Minerals Corporation, Lucerne Valley, CA) and dolomite (with 0.1–1.0 percent (wt/wt) quartz and 0.1–1.0 percent (wt/wt) tremolite, density of 2.78 g/cm^3; Specialty Minerals Corporation, Canaan, CT) sands were sieved, and the 250 to 355 μm size fraction was retained for the measurements (in later capillary scaling analyses, we set the characteristic grain size λ to the median grain size of 302 μm). All the sieved minerals were rinsed several times in deionized (DI) water only to remove finer particles and possible loosely attached impurities. In order to best preserve the original properties of the minerals and closely simulate natural porous media, no aggressive chemical or physical cleaning (e.g., acetone, ethanol or acid washing, plasma, sonication) was performed. After cleaning, the minerals were dried in oven at 110–120 ºC.

Pre- and post-experiment analysis of materials including scanning electron microscope (SEM), X-ray diffraction (XRD) and Brunauer, Emmett and Teller (BET) specific surface area measurements were conducted. SEM (Zeiss Gemini Ultra-55) images were taken to examine surface morphology and roughness of the sand particle samples at nm to μm scale. Prior to imaging, the sand grains were sputter-coated with gold. As shown in Figure S1, quartz sands are generally well-rounded while limestone sands are more angular. Comparing fresh sands with aged sands during experiments in $scCO_2$ saturated brine, insiginificant changes were observed.

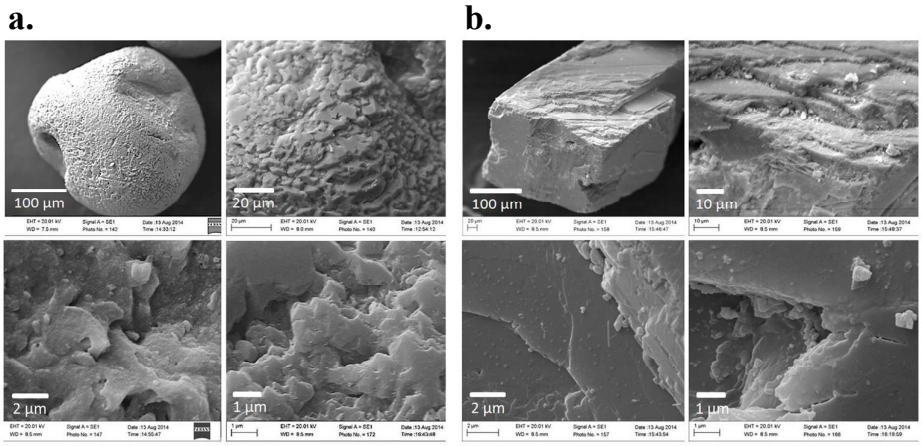

Figure S1. Scanning electron microscope (SEM) images of (a) Quartz (SiO_2) and (b) Limestone ($CaCO_3$) sands.

XRD measurements were conducted on quartz, limestone and dolomite sand samples to determine mineral contents. Mineralogical compositions were identified using powder XRD (Rigaku SmartLab X-ray Difractormeter). As shown in Figure

S2, the sand samples used in this study are representative with quartz, limestone and dolomite being the dominant minerals, respectively.

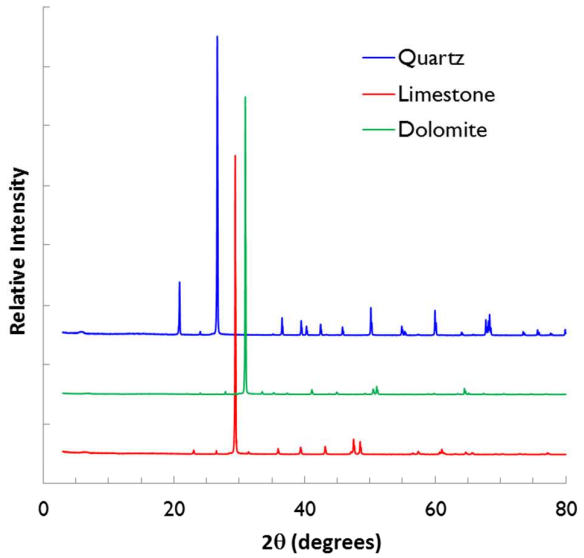

Figure S2. X-ray diffraction (XRD) diagrams of Quartz (SiO_2), Limestone ($CaCO_3$) and Dolomite ($CaMg(CO_3)_2$) sands, showing sample mineralogy.

BET measurements were conducted on quartz, limestone and dolomite sands to determine specific surface area, pore size distribution and porosity. The specific surface areas of the samples were measured on an Autosorb-1 surface area analyzer (Quantachrome Instruments) with Krypton (Kr) as the adsorption gas. Prior to the measurements, samples were degassed under vacuum at 150 ˚C for 3 hours to remove any moisture and adsorbed gas. Surface areas were calculated according to 5 points BET measurements at a relative pressure ranging from 0.05 to 0.3 P/P_0 using the classic BET equations. As shown in Table S1, quartz sand has a specific surface area that is about 4 times of that of the carbonate sands. The low specific surface areas, especially for the carbonates show that these sands have insignificant internal porosity.

Table S1. Brunauer, Emmett and Teller (BET) Specific Surface Area Measurements on Quartz (SiO_2), Limestone ($CaCO_3$) and Dolomite ($CaMg(CO_3)_2$) Sands with Kr as the Adsorption Gas.

Sample	Kr-BET specific surface area, m^2/g	r, correlation coefficient
Quartz	0.103	0.9994
Limestone	0.028	0.9999
Dolomite	0.032	0.9998

2 Fluids

In our experiments, clean CO_2 from a cylinder (99.99% purity, Airgas) was pressurized inside the high pressure syringe pump (500D HP, Teledyne Isco Corp., rated to 34.5 MPa) to its supercritical states under 8.5 and 12.0 MPa, representing reservoir conditions at depths of about 0.85 and 1.2 km. We conducted our own $scCO_2$–brine interfacial tension (γ) measurements using the pendant drop method,[1] under the same conditions for the P_c–S_w experiments. Our measured values are included in Table S2, along with γ measurements from the literature obtained under similar conditions for comparison.

Table S2. Pressure and Temperature Dependent Fluid and Interfacial Properties under Our Experimental Conditions.

Temperature	˚C	23.5	45	45
Pressure	MPa	0.1	8.5	12.0
1.0 M NaCl brine density, ρ_w	$kg \cdot m^{-3}$	1036[a]	1032[a]	1034[a]
Nonaqueous fluid phase		air	$scCO_2$	$scCO_2$
Nonaqueous fluid density, ρ_n	$kg \cdot m^{-3}$	1.2	282[b]	658[b]
ρ_w-ρ_n	$kg \cdot m^{-3}$	1035	750	376
$(\rho_w$-$\rho_n)g$	$kg \cdot m^{-2} \cdot s^{-2}$	10153	7358	3689
$(\rho_w$-$\rho_n)g(H/2)$	Pa	152.3[c]	73.6[c]	36.9[c]
Fluid–fluid interfacial tension	$mN \cdot m^{-1}$	74.4[d]	33.1±0.5[e]	30.1±0.4[e]
Regression for NaCl/KCl brine[5]			39.1[f]	35.1[f]
76 g/L synthetic brine (~1 M NaCl)[1]			32.7[g]	25.5[g]
0.87 M NaCl, interpolated T[6]			33[h]	28[h]

[a]The NaCl brine densities were calculated based on the regression equations of Batzle and Wang.[2]

[b]$scCO_2$ densities were obtained from CO_2 phase diagram in the National Institute of Standards and Technology (NIST) web-based database (http://webbook.nist.gov/chemistry/fluid/).[3]

[c]The $(\rho_w$-$\rho_n)g(H/2)$ values represent magnitudes of variations in P_c relative to the value at the horizontal midplane of the sandpack, associated with ±0.01 m (half the sample height, H= 0.02 m) for $scCO_2$ and ±0.015 m (H= 0.03 m) for air under hydrostatic equilibrium condition.

[d]Interfacial tension value for 1.0 M NaCl air-brine is from *Weast*.[4]

[e]Interfacial tensions for $scCO_2$–brine were measured in our laboratory using the pendant drop method.[1]

[f]Estimated interfacial tensions for experiments with $scCO_2$ were obtained by applying the regression relations by *Li et al.*,[5] assuming equivalence our NaCl solutions with a solution of monovalent ions comprised primarily of NaCl (86.4%, with 13.6% KCl).

[g]Interfacial tensions for a $scCO_2$–brine system with a 76 g/L brine (compared to our 1 M NaCl=58 g/L), at 8 (versus our 8.5) and 12 MPa, 41˚C, from *Bachu and Bennion*.[1]

[h]Interpolated values (measurements at 27˚C and 71˚C) for 0.87 M NaCl by *Chalbaud et al.*[6]

3 High Pressure Sample Chamber

The limestone sand sample resided inside a stainless steel chamber (rated to 20.7 MPa). The configuration of the high pressure sand column chamber is shown in Figure S3. A 316 stainless steel porous plate (5 μm pore size for 12 MPa tests and 2 μm for 8.5 MPa tests, 3.0 mm thick, 104.8 mm diameter, Mott Corp.) was fitted into the slot between the top and bottom cavity of the custom built high-pressure vessel (Parr Instrument Co.). The stainless steel ring (internal diameter 82.1 mm, height H = 20 mm) which contains the sand was placed on top of the porous plate. The limestone sand samples were wet-packed with the brine inside the ring to complete WP saturation at φ = 0.38 (pore volume 42.1 mL). Permeability measurements with 1.0 M NaCl brine obtained on a separate sample of the sand (packed to the same φ) yielded a k of 3.9×10^{-11} m^2 (hydraulic conductivity of 3.9×10^{-4} m·s^{-1}). Equilibrium P_c at each height h relative to the midplane was calculated by $(\rho_w-\rho_n)gh$. A stainless steel spacer (40 mm thick, 94.7 mm diameter) with 24 flow conduits (3.0 mm diameter) sat on top of the sandpack to compensate the void space volume inside the chamber and to prevent displacement of the sand during pressurization. Buna-N O-rings were used between all the aforementioned parts to ensure that inflow and outflow only occurred through the sandpack and the stainless steel porous plate. A graphite gasket was used in the reactor lid to provide leak-proof sealing and minimize possible contamination. A rupture disc (rated to 20 MPa, Fike Corp.) on the reactor's cap ensured safe venting in the event of accidental over-pressurization. After the chamber was capped with the reactor lid, it was tightened with the bolts of a split ring assembly.

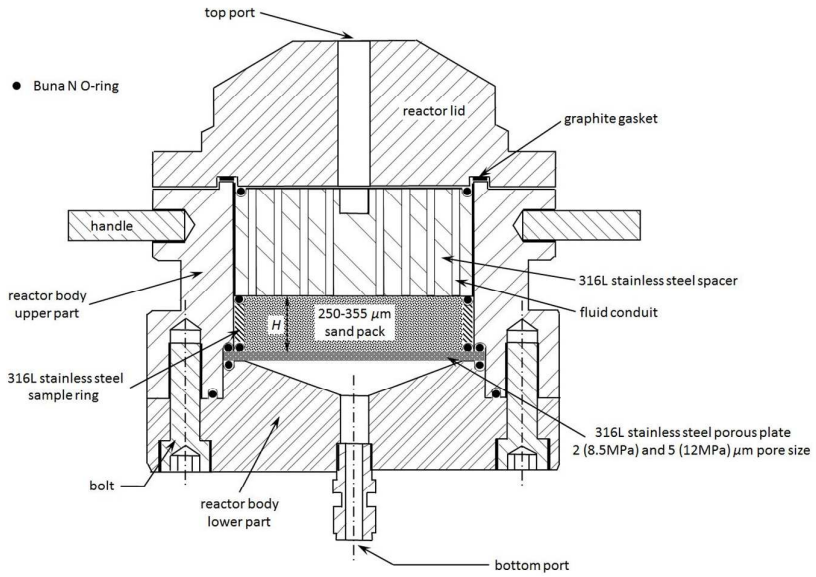

Figure S3. High-pressure sample chamber (drawing adapted from original drawing by Parr Instrument Co.). A custom-built high-pressure reaction vessel (Parr Instrument Co.) served as the body of the chamber, with additional components placed in its cavity. The reactor lid is sealed into place with bolts on a pair of split ring clamps (not shown).

4 High Pressure P_c—S_w System

The exterior and interior of the high pressure P_c–S_w system is shown in Figure S4. P_c is precisely controlled via a high pressure sight glass P_c regulator whose height is set by a computer-programmed automatic linear actuator. Constant system temperature is maintained by housing all the components of this system inside a thermally insulated enclosure.

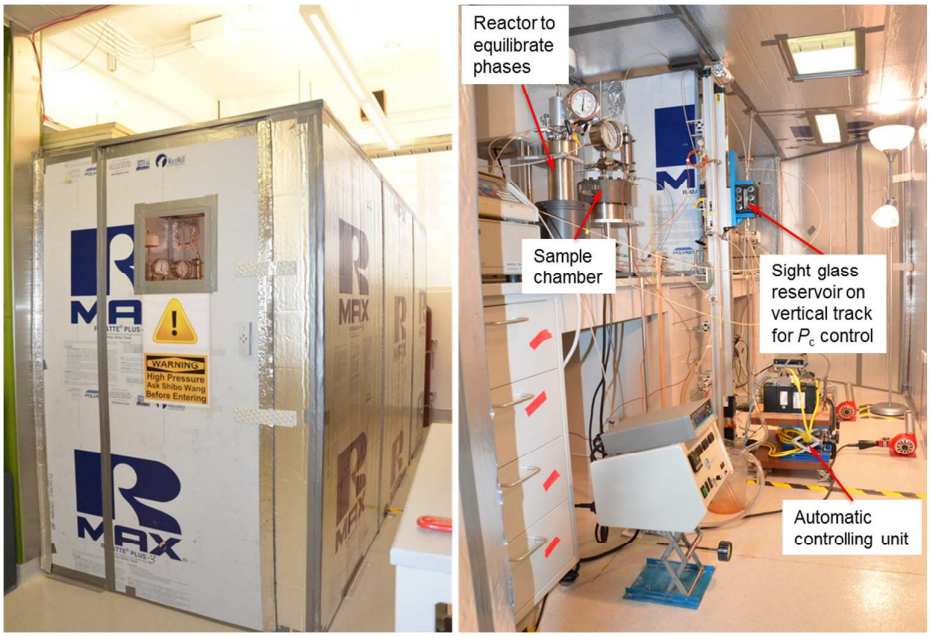

Figure S4. Pictures of the exterior (Left) and interior (Right) of the high pressure P_c–S_w measurement system. The main and back-pressure ISCO pumps are not visible in the picture.

5 Experimental Procedure

Before use, the equipment including the syringe pumps, the high pressure cylinder, the sight glass vessel, the porous plates, the sample chambers, valves, connectors, tubing and all the other components used in the ambient pressure and elevated pressure experiments were well cleaned with acetone/ethanol first, then extensively rinsed with DI water and finally flushed with clean air.

5.1 ETP Experiments for $scCO_2$—Brine

As many of the preparatory steps in the ETP experiments as possible are done at room temperature. It should be noted that later initialization and adjustment steps conducted by working within the thermally insulated enclosure must be done quickly to ensure that heat related health risks are avoided.

Before experiments, about 350 mL brine was added into a stirred high-pressure reactor vessel (4562 Mini Reactor system, Parr Instrument Co., 450 mL, rated to 20 MPa) to prepare brine-saturated $scCO_2$ and $scCO_2$-saturated brine. Liquid CO_2 from the bottom of the CO_2 cylinder via eductor tube was dispensed into the main syringe pump. $scCO_2$ was prepared in the syringe pump and then pumped into the stirred reactor where $scCO_2$ and brine were mixed to phase equilibrium for at least

48 hours before use. Leak test was carefully conducted at all the ports and valve and tubing connections to ensure the system is leak proof.

When an ETP experiment started, brine-saturated $scCO_2$ from the stirred reactor was first added into the sample chamber through the upper port #1 (connected with the stirred reactor) to fill up the void space on top of the sandpack and the system's total pressure was maintained at the target value by the main syringe pump. The valve at the upper port #1 was then closed and the valve at the lower port, which connected the stirred reactor and the sample chamber, was opened. The valve at the upper port #2 (connected with the high pressure cylinder prefilled with $scCO_2$ via the back pressure syringe pump) in the sample chamber was opened and the $scCO_2$-saturated brine was pumped into the sample chamber from the bottom. The fresh brine in the sand column was thus discharged into the cylinder and the flushing (replacing the fresh brine from the wet-packing with $scCO_2$-saturated brine) of the sample column ensued under the pressure differential between the main and backpressure syringe pumps. The sample chamber was purged with at least 3 pore volumes of $scCO_2$-saturated brine at a rate of about 1–5 mL/min. In this way, the sandpack was set to be fully saturated with the WP (i.e., the $scCO_2$-saturated brine). After the flushing was done, the sample chamber was temporarily isolated from the main loop. Brine-saturated $scCO_2$ from the stirred reactor was filled into the high-pressure P_c–S_w controller/meter. Next, a small amount of $scCO_2$-saturated brine was introduced into the high-pressure P_c–S_w controller/meter in order to bring the $scCO_2$-brine meniscus into view at the bottom portion of the window (by means of the back-pressured cylinder). The vertical position of the high-pressure P_c–S_w controller/meter was adjusted such that the elevation of the $scCO_2$–brine interface coincided with the center of the sand pack. This starting condition for P_c–S_w measurements corresponds to an average P_c = 0 Pa. Finally, the respective top and bottom valves of the sample chamber and the sight glass vessel were connected, forming a hydraulically closed loop. This loop was linked to the main syringe pump at the upper port #1 of the sample chamber to maintain the target experimental total pressures (8.5 or 12.0 MPa). The entire system was left for equilibration for at least 24 hours prior to data collection. It should be noted that the P_c values represent conditions at the horizontal midplane of the sand sample, and that variations within the column can be as large as ±73.6 Pa for 8.5 MPa and ±36.9 Pa for 12.0 MPa relative to the midplane value under the influences of gravity and fluid densities (Table S2).

It should be noted that in the drainage–imbibition experiments, P_c was changed successively with many equilibration steps while in the separate $S_{nw,r}$ vs $S_{nw,i}$ experiments, positive (drainage) and negative (imbibition) P_c was set with only one equilibration step (i.e., from midplane to desired position for $S_{nw,i}$ equilibration during drainage and from the equilibrated $S_{nw,i}$ position directly back to midplane).

5.2 RTP Experiments for Air–Brine

In the air–brine experiments on limestone and dolomite sands under RTP conditions, experimental procedures were in the most part similar to the ETP experiments except for the laborious operations of pressure and temperature maintenance, fluid flushing and backpressure control. A plastic column (92 mm diameter, height H = 30 mm, Soilmoisture Equipment Corp.) with a ceramic porous plate (0.05 MPa capillary pressure threshold, 12.7 mm thick, 92 mm diameter, Soilmoisture Equipment Corp.) was employed. The sand samples were carefully wet-packed to full brine saturation (φ = 0.38, pore volume 63.0 mL, k = 3.9×10^{-11} m^2) inside the plastic column. The bottom port of the plastic chamber was connected via polyethylene (PE) tubing to the bottom end of a vertically oriented 50 mL serological pipette (labeled in 1 mL increments, volumes resolution to 0.2 mL, VWR International Corp.). The pipette served the same purpose as the graduated sight glass in the ETP experiments (i.e., capillary pressure regulator through adjusting the elevation of the air–brine interface relative to the sample center as well as a reservoir for measuring outflow/inflow from the sample). The top port of the plastic column and the upper portion of the pipette were both vented to the room air (and thus local atmospheric pressure). After wet-packing the sample, the brine level in the pipette was adjusted to a position within the bottom portion of the pipette (low volume reading), and hydrostatically equilibrated at the horizontal midplane of the sand pack for at least 24 hours before measurements. This configuration allowed equilibration to an average P_c = 0, with a variation within the sand pack of $\pm(\rho_w-\rho_n)g(H/2)$, which amounted to ±152 Pa within the 30 mm column (Table S2). It also enabled fine control of P_c by setting the level of the air–brine interface in the pipette at the desired elevation as was previously described in the $scCO_2$–brine experiments. Drainage curves were obtained by successively moving the air–brine interface in the pipette downward to lower depths, h, relative to the horizontal midplane of the sand pack and recording outflow volumes.[7] Imbibition curves were obtained by reversing this procedure through a series of stepwise equilibrations, returning to P_c = 0. Time intervals of 1 to 2 days between equilibration steps were used depending on the stage of drainage/imbibition. Primary and duplicate/secondary cycles of drainage and rewetting were conducted.

6 Results

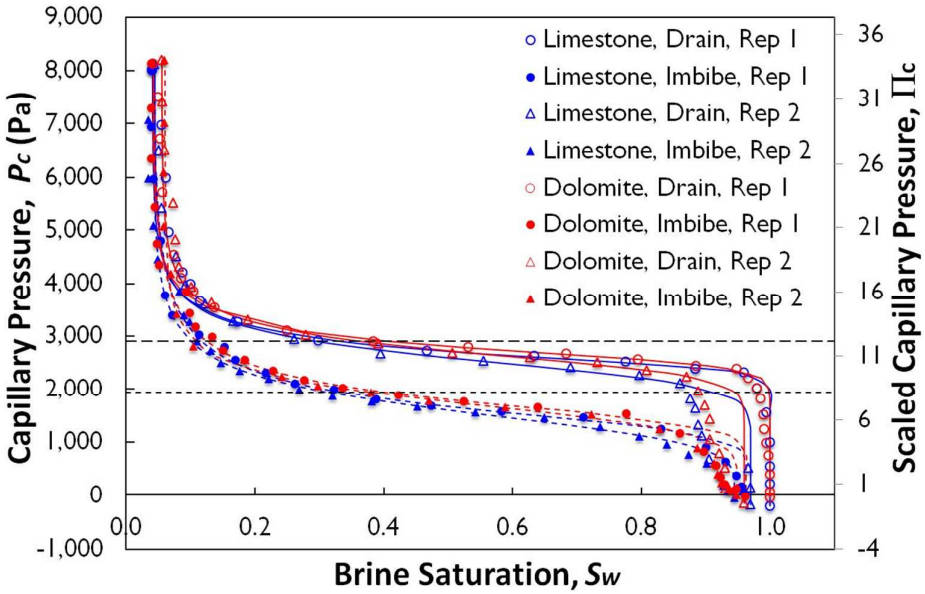

Figure S5. P_c–S_w relations during drainage and imbibition/rewetting in limestone and dolomite sands at RTP. Experiments involving duplicate drainage–imbibition cycles were conducted. The sandpacks were saturated with brine (i.e., $S_{w,i} = 1.0$ and $V_w/V_b = 0.38$) prior to the initial drainage cycle. Unscaled P_c-S_w and capillary-scaled with grain size and IFT ($\Pi_c = \lambda P_c/\gamma$) Π_c–S_w relations are presented in the same plot. Universal values of Π_c inflection points (~12 for drainage and ~8 for imbibition, noted by the dash lines) are included for comparisons. Values of γ used in capillary scaling are listed in Table S2. The continuous curves are the fitted data based on van Genuchten model[8] in the nonlinear regression analysis. The fitting parameters are summarized in Table S3 and scaling inflections are presented in Table S4. "Rep" = Replicate.

Table S3. Curve Fitting Parameters of van Genuchten Model (Equation 3) to Drainage and Imbibition Curves (Figure S5 and 2)[a]

		Θ_s	S_s	Θ_r	S_r	α (Pa^{-1})	n	m
Air–limestone–1	Drainage	0.380	1.00	0.015	0.04	4.09×10^{-4}	26.85	0.26
	Imbibition	0.366	0.96	0.015	0.04	7.15×10^{-4}	7.50	0.45
Air–limestone–2	Drainage	0.369	0.97	0.017	0.04	4.09×10^{-4}	10.30	0.68
	Imbibition	0.359	0.94	0.015	0.04	6.32×10^{-4}	4.60	0.95
Air–dolomite–1	Drainage	0.380	1.00	0.015	0.04	3.91×10^{-4}	21.45	0.35
	Imbibition	0.366	0.96	0.015	0.04	6.54×10^{-4}	8.64	0.43
Air–dolomite–2	Drainage	0.365	0.96	0.021	0.06	3.95×10^{-4}	12.98	0.55
	Imbibition	0.361	0.95	0.023	0.06	5.67×10^{-4}	5.61	1.03
8.5 MPa CO_2–fresh limestone	Drainage	0.380	1.00	0.021	0.06	4.22×10^{-4}	6.47	33.62
	Imbibition	0.366	0.96	0.021	0.06	4.47×10^{-5}	8.35	0.30
8.5 MPa CO_2–1.5 months aged limestone	Drainage	0.380	1.00	0.020	0.05	9.41×10^{-4}	4.96	2.48
	Imbibition	0.340	0.89	0.020	0.05	4.01×10^{-3}	7.44	0.46
12.0 MPa CO_2–fresh limestone	Drainage	0.380	1.00	0.015	0.04	1.59×10^{-3}	19.24	0.47
	Imbibition	0.284	0.75	0.015	0.04	1.06×10^{-3}	2.25	33.61
12.0 MPa CO_2–1.5 months aged limestone	Drainage	0.380	1.00	0.016	0.04	2.54×10^{-3}	46.82	0.13
	Imbibition	0.339	0.89	0.015	0.04	5.74×10^{-4}	2.30	74.64
12.0 MPa CO_2–4 months aged limestone	Drainage	0.380	1.00	0.028	0.07	1.71×10^{-3}	3.92	2.61
	Imbibition	0.263	0.69	0.028	0.07	1.76×10^{-2}	3.27	0.58

[a]Note that curves were fitted to minimize root-mean-square deviations to the full drainage or imbibition curves instead of forcing through data at $P_c = 0$.

Table S4. Calculated Inflection Matric Heads from Capillary Scaling and Experimental Inflection Matric Heads from Measurements. w and θ Values that Satisfactorily Match Our Experimental Results with the Universal Scaling Inflections at RTP, 8.5 and 12.0 MPa are Listed, Respectively.

		Theoretical inflection head, cm	Experimental inflection head, cm	Experimental scaled inflections	Advancing/receding contact angle θ, °	w ($\approx\cos\theta$)
Air—limestone—1	Drainage	29.1	26.3	11.1	23.0	0.92
	Imbibition	19.4	16.2	6.8	32.0	0.85
Air—limestone—2	Drainage	29.1	25.3	10.6	28.0	0.88
	Imbibition	19.4	15.8	6.6	34.0	0.83
Air—dolomite—1	Drainage	29.1	27.6	11.6	15.0	0.97
	Imbibition	19.4	17.8	7.5	20.0	0.94
Air—dolomite—2	Drainage	29.1	26.9	11.3	20.0	0.94
	Imbibition	19.4	17.0	7.1	27.0	0.89
8.5 MPa CO_2—fresh limestone	Drainage	17.9	17.8	11.9	7.0	0.99
	Imbibition	11.9	4.0	2.7	70.5	0.33
8.5 MPa CO_2—1.5 months aged limestone	Drainage	17.9	11.6	7.8	49.5	0.65
	Imbibition	11.9	4.0	2.7	70.5	0.33
12.0 MPa CO_2—fresh limestone	Drainage	32.4	18.1	6.7	56.0	0.56
	Imbibition	21.6	4.5	1.7	78.0	0.21
12.0 MPa CO_2—1.5 months aged limestone	Drainage	32.4	11.8	4.4	68.6	0.36
	Imbibition	21.6	6.6	2.4	72.3	0.30
12.0 MPa CO_2—4 months aged limestone	Drainage	32.4	11.8	4.4	68.6	0.36
	Imbibition	21.6	1.9	0.7	85.0	0.09

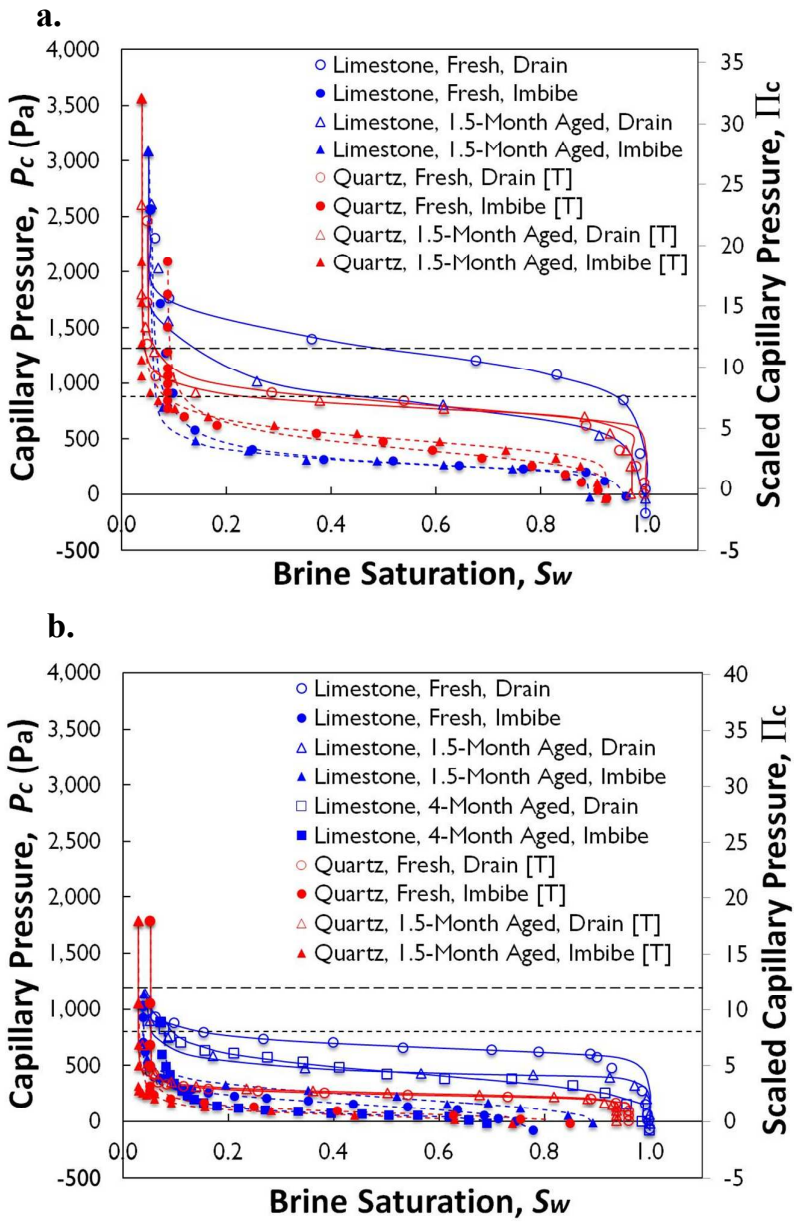

Figure S6. P_c–S_w relations during drainage and imbibition in limestone and quartz sands with $scCO_2$ at (a) 8.5 and (b) 12.0 MPa, 45 ˚C. Capillary-scaled Πc dependence on brine saturation was also presented with universal scaling inflections (straight dash lines) included for comparison. The data were fit with the van Genuchten model.[8] The data of quartz were from previous study[9] and were denoted as [T] in the figures.

7 References

1. Bachu, S.; Bennion, D. B. Interfacial tension between CO_2, freshwater, and brine in the range of pressure from (2 to 27) MPa, temperature from (20 to 125) degrees C, and water salinity from (0 to 334 000) mg L^{-1}. *Journal of Chemical and Engineering Data* **2009**, *54*(3), 765–775.

2. Batzle, M.; Wang, Z. Seismic properties of pore fluids. *Geophysics* **1992**, *57*(11), 1396–1408.

3. National Institute of Standards and Technology (NIST) web-based database: http://webbook.nist.gov/chemistry/fluid/. as of April 2015.

4. Weast, R. C. CRC Handbook of Chemistry and Physics, 58 ed. **1977**, F-43, CRC Press, Cleveland, Ohio.

5. Li, X.; Boek, E.; Maitland, G. C.; Trusler, J. P. M. Interfacial tension of (brines+CO_2): 0.864 NaCl + 0.136 KCl) at temperatures between (298 and 448) K, pressures between (2 and 50) MPa, and total molalities of (1 to 5) mol kg^{-1}, *Journal of Chemical and Engineering Data* **2012**, *57*(4), 1078–1088.

6. Chalbaud, C.; Robin, M.; Lombard, J.-M.; Bertin, H.; Egermann, P. Brine/CO_2 interfacial properties and effects on CO_2 storage in deep saline aquifers. *Oil and Gas Science and Technology* **2010**, *65*(4), 541–555.

7. Tokunaga, T. K.; Wan, J.; Olson, K. R. Saturation-matric potential relations in gravel. *Water Resources Research* **2002**, *38,* 1214.

8. van Genuchten, M. T. A closed-form equation for predicting the hydraulic conductivity of unsaturated soils. *Soil Science Society of America Journal* **1980**, *44*(5), 892-898.

9. Tokunaga, T. K.; Wan, J.; Jung, J. W.; Kim, T. W.; Kim, Y.; Dong, W. Capillary pressure and saturation relations for supercritical CO_2 and brine in sand: High-pressure $P_c(S_w)$ controller/meter measurements and capillary scaling predictions. *Water Resources Research* **2013**, *49*(8), 4566-4579.